ISSN 0915-633X

NATIONAL INSTITUTE FOR FUSION SCIENCE

On Radial Electric Field Structure in CHS Torsatron/Heliotron

H. Sanuki, K. Itoh, K. Ida and S.-I. Itoh

(Received – May 10, 1991)

NIFS-94 Jun. 1991

RESEARCH REPORT
NIFS Series

NAGOYA, JAPAN

On Radial Electric Field Structure in CHS Torsatron/Heliotron

H. Sanuki, K. Itoh, K. Ida and S.-I. Itoh

National Institute for Fusion Science, Nagoya, 464-01, Japan

Abstract

The radial electric field structure in helical system is discussed taking into account the effects of the orbit loss and charge exchange loss in addition to the neoclassical fluxes. Analysis is made for the CHS torsatron/heliotron, in which the radial electric field E_r was estimated experimentally. It was found that the fast ion orbit loss and charge exchange loss have strong influence on the profile of the radial electric field, particularly near the plasma periphery. The absolute value of E_r in the experiments is still more negative than the theoretical prediction.

KEYWORDS : radial electric field, CHS torsatron/heliotron, Neoclassical, fast ion orbit loss, charge exchange loss

§1 Introduction

Recently, it has been widely recognized that the radial electric field E_r near the plasma edge plays an important role on the improved confinement such as in the H-mode[1-3]. Theoretical prediction that the bifurcation in the radial electric field causes the H/L transition has been made[4], and theories have followed that the gradient of the radial electric field ($\partial E_r/\partial r$) has a strong influence on the suppression of microinstabilities and is expected to reduce anomalous transports[5-11]. Experiments on many tokamaks have confirmed the rapid change of the radial electric field and strong inhomogeneity of it[2,3,12,13], although, strictly speaking, the causality between the transition and E_r has not been experimentally established. In Torsatron/Heliotron stellarators, the neoclassical theory predicts that an electric field reduces the helical ripple loss and improves the confinement[14,15]. Therefore, the detailed measurement of the electric field and their gradient is one of the key topics in helical systems as well as in tokamaks.

In the Wendellstein VII-A stellarator and Heliotron-E devices[16,17], the poloidal rotation has been measured only near the plasma periphery, using the intrinsic impurity radiation. It has been discussed that a large negative electric field ($E_r \sim -450$V/cm) was built up by the fast ion loss of perpendicularly-injected neutral beams in Wendellstein VII-A. This is considered to be originated from the fact that a significant loss cone for ions exists due to the large aspect ratio and the moderate rotational transform. Quantitative comparison of the theory and

experiments on E_r profiles is far from satisfactory. Since a neutral beam is injected tangentially in the Compact Helical System (CHS)[18], however, the fast ion loss may become less significant and the many mechanisms involved would be important in determining the radial electric field. Recent measurements on the poloidal and toroidal rotations in CHS[19], by using the charge exchange spectroscopy (CXS)[20], have covered the whole region from the axis to the edge, thus providing the radial profile in the plasma column.

In this article, we discuss a theoretical model to determine the radial electric field and compare the results with experimental observations. The roles of the fast ion orbit loss and charge exchange are investigated. It is found that these processes, which is not included in the neoclassical theory, make E_r near edge more negative. This influence is considerable, but still is not enough to explain the experimental observations.

In section 2, the experimental results of the electric field in tangential NBI experiments in CHS device are briefly described. A theoretical model to determine an electric field is discussed in §3. The evaluation of E_r and comparison with the experimental results are given in §4. The last section is devoted to the summary and discussions.

§2 Brief Survey of Experimental Results

The CHS device is a Torsatron/Heliotron configuration (multipolarity ℓ=2, and toroidal pitch number m=8), with a major radius of 100cm and an average minor radius of 20cm. The toroidal magnetic field B_t is 1T. We use the coordinates (r, θ, ϕ) where r is the minor radius, θ is the poloidal angle and ϕ is the toroidal angle.

The electron temperature and density profiles, $T_e(r)$ and $n_e(r)$, are measured with Thomson scattering. The ion temperature and poloidal as well as toroidal rotation velocity profiles, $T_i(r)$, U_θ and U_ϕ, are measured by CXS. Radial electric field profiles are evaluated by using the force balance equation for impurities

$$E_r = (\partial P_I/\partial r)/eZ_I n_I - (B_\theta U_\phi - B_\phi U_\theta), \qquad (1)$$

where the suffix I stands for the measured impurity species. It should be noted that the radial frictional force between different species is small enough to be neglected.

For the NBI discharges in CHS, as is shown in previous articles[19,21,22], the toroidal rotation velocity is damped at r>0.3a by the strong parallel viscosity caused by the helical ripple[22]. The poloidal rotation has a strong shear near the plasma edge. The poloidal rotation velocity shear results from the inhomogeneity of the radial electric field near the plasma periphery. It was also found that the poloidal rotation velocity at the plasma edge depends on the collisionality.

To simplify the following analysis, the magnetic field structure is fitted to the conventional torsatron configuration with one helical harmonic as

$$B = B_0[1-\varepsilon_t(r)\cos\theta-\varepsilon_h(r)\cos(\ell\theta-m\phi)], \tag{2-1}$$

$$\varepsilon_t(r) = r/R, \tag{2-2}$$

and

$$\varepsilon_h(r) = \ell\varepsilon_0 I_\ell(mr/R), \tag{2-3}$$

where I_ℓ is a modified Bessel function of the first kind, and the constant ε_0 is 0.3919 for the discharges subject to the analysis. This simplification gives the form of the rotational transform ι as

$$\iota(r) = \frac{1}{2}\epsilon_0^2\frac{Rl^3}{r}\frac{d}{dx}\left(\frac{I_l}{x}\frac{dI_l}{dx}\right), \tag{3}$$

where x=mr/R and the safety factor is given by q(r)=1/ι. This fitting does not includes the positive pitch modulation of the helical winding with α^*=0.3 in CHS device. The effect of α^* was examined in Ref.[19]; it was confirmed that the α^* effect slightly changes E_r near edge but is far insufficient to explain experiments.

§3 A Theoretical Model to Determine E_r

In this section, we consider a theoretical model to explain the large electric field measured near the plasma edge. We study the steady state solution of the ambipolarity equation, taking into account nonclassical terms as

$$\Gamma_i = \Gamma_i^{NC(s)} + \Gamma_i^{NC(as)} + \Gamma_i^{orbit} + \Gamma_{fcx} + \Gamma_{icx}. \qquad (4)$$

This equation consists of the neoclassical fluxes (denoted by the superscript of NC), the fast ion orbit loss flux (Γ_i^{orbit}), the charge exchange contributions of fast ions (Γ_{fcx}) and bulk ions (Γ_{icx}). The orbit loss of bulk ions are not taken into account, because the bulk ions are not in the collisionless regime for the discharges of our interest. The neoclassical contribution is given as the sum of the flux $\Gamma_i^{NC(s)}$, associated with the passing and toroidally trapped particles, and $\Gamma_i^{NC(as)}$ related to the ripple trapped particles, according the Ref.[14]. For electrons, the nonclassical terms in Eq.(4) are insignificant. Only the neoclassical terms are kept in the electron flux.

The explicit form of the fast ion orbit loss is discussed in Appendix A. It follows that

$$\Gamma_i^{orbit}(r) \simeq \frac{1}{4\pi^2 R r}\frac{P_{in}}{E_b}\left(\frac{r-r_*}{a-r_*}\right) f_{bound}, \qquad (5)$$

where P_{in} is the input power, E_b denotes the beam energy, r_* is the radius representing the loss boundary, and the coefficient f_{bound} implies the fraction of the power absorbed in the region

$r_* < r < a$. The dependence of the radius r_* on the radial electric field was discussed and expression is given in Ref.[23].

The fast particle flux is generated by the charge exchange loss. The charge process conserves a local charge, but takes away the momentum. This loss of momentum causes the drift flux in the radial direction. Simplifying that the fast particle velocity is characterized by the toroidal one with injection energy, the toroidal momentum density of fast particles is given as $M_f n_f v_f$, where M_f is the fast ion mass, $n_f(r)$ is the fast ion density and $v_f = \sqrt{2E_b/M_f}$. The rate of the charge exchange with neutral particles is $n_0\langle\sigma v_f\rangle$, and the toroidal force on fast ions associated with the cx loss is evaluated as

$$F_t = -n_0\langle\sigma v_f\rangle M_f n_f v_f, \tag{6}$$

where $n_0(r)$ is the neutral particle density. Balancing this force with the toroidal force $e\Gamma_{fcx}B_p/c$, we have

$$\Gamma_{fcx} \simeq \frac{c}{eB_p} M_f n_f n_o < \sigma v_f > v_f, \tag{7}$$

The cross section $\langle\sigma\rangle$ is approximated by the formula[24]

$$< \sigma > = \frac{0.6937 \times 10^{-18}(1 - 0.155\ log_{10}E_b)^2}{1 + 0.1112 \times 10^{-14}E_b^{3.3}}[m^2], \tag{8}$$

The cx rate $\langle\sigma v\rangle$ is estimated at the energy of the fast ion.

The charge exchange of bulk ions with neutrals can cause the radial electric field. The momentum loss rate is calculated in tokamaks, which in turn gives the radial ion flux through the

force balance. In tokamaks, the toroidal force balance is used[6,7,25], because the bulk ion viscosity directs in the poloidal direction[26]. In helical systems, the toroidal rotation damps off due to the large helical ripple and the poloidal flow remains[26]. Since we are interested in the region r/a>0.3, we assume that the main ions are rotating in the poloidal direction and subject to the poloidal force due to the cx loss. The induced radial flux by this poloidal force is

$$\Gamma_{icx} = \frac{c}{eB_t} nM < \sigma v_i > n_o u_p, \tag{9}$$

where M is the ion mass, and the cx cross section is estimated with the energy of bulk ion temperature. The poloidal velocity is given as

$$u_p = -\frac{cT_i}{eB_t}[-\frac{eE_r}{T_i} + \frac{1}{n}\frac{dn}{dx} + (1+\frac{\mu_{i2}}{\mu_{i1}})\frac{1}{T_i}\frac{dT_i}{dx}], \tag{10}$$

where μ_{i1} and μ_{i2} are neoclassical viscosity coefficient.

The radial electric field solution in the steady state is evaluated by the ambipolarity equation

$$\Gamma_i = \Gamma_e^{NC}. \tag{11}$$

This equation is a nonlinear algebraic equation with respect to the radial electric field if one employs the formula of Ref.[14]. Equation (11) can have multiple solutions on each magnetic surface. This equation is given on each magnetic surface, and contains a class of solutions $E_r(r)$ which have discontinuities at

some radial points. This fundamental solution to the problem of the discontinuity can be given by noticing the small but finite diffusion coefficient of the radial electric field[28]. We therefore look for the solution which is continuous and satisfies the condition

$$E_r(r) \to 0 \text{ as } r \to 0. \tag{12}$$

§4 Evaluation of Radial Electric Field

In this section we estimate the radial electric field from the ambipolar condition Eq.(12) with the experimentally obtained plasma profiles. To study the collisionality dependence, two typical NBI discharges, namely, the low density and high density discharges, are studied.

In order to use the experimental data in the analysis, the following fittings are used. As for the bulk plasma parameters, we use

$$n(\rho) = (n(0)-n_s)\frac{(1-\rho^{\alpha_2})}{\gamma}[1-(1-\gamma)(1-\rho^{\alpha_2})^{\beta_2-1}]+n_s, \tag{13}$$

$$T_e(\rho) = (T_e(0)-T_{es})(1-\rho^{\alpha_3})^{\beta_3}+T_{es}, \tag{14}$$

and

$$T_i(\rho) = (T_i(0)-T_{is})(1-\rho^{\alpha_4})^{\beta_4}+T_{is}, \tag{15}$$

where ρ is the normalized radius r/a, and the indices (α_k, β_k) are constant (k=2-4). The coefficient γ is introduced to fit the hollow profile, and is given as $\gamma = 1-\beta_2^{-1}[1-\rho_m^{\alpha_2}]^{(1-\beta_2)}$. ρ_m is the minor radius corresponding to the maximum of the density. n_s and T_s represent the values at the plasma edge. Simplified form is employed for fast ions and neutral particles. We assume that n_0 and n_f profiles are given

$$n_0(\rho) = n_{0s}\exp[-\alpha_0(1-\rho)^2], \tag{16}$$

and

$$n_f(\rho) = n_{f0} \exp[-\alpha_1 \rho^2], \tag{17}$$

where n_{0s} is the neutral density at edge, and n_{f0} is the fast ion density at the center. Parameters α_0 and α_1 are constants.

The characteristic parameters, which are adjusted so as to reproduce the experimental results, are listed in Table 1 for the low density and high density NBI discharges. Since the accurate experimental data are not available for the neutral and fast particles, we employ plausible values for n_{0s}, n_{f0}, α_0 and α_1. The best fitting curves for the profiles of the density and temperature are plotted in Fig.1A (low-density) and in Fig.1B (high-density) for two cases shown in Table 1. This choice of the fast particle density gives the heating rate of about $1MW/m^3$, which is in the range of experiments.

We first review the result of the neoclassical estimate. Figure 2 illustrates Γ_j^{NC} (j=i,e) as a function of E_r for the position of ρ=0.8. Dashed lines are for the case of the low density, and the solid ones are for the high density case. The solution of the ambipolarity condition is denoted by an open circle. Solution of the equation $\Gamma_i^{NC}=\Gamma_e^{NC}$ with the condition Eq.(12) was compared with experimental observations[19]. The experimental observations show that the neoclassical estimations are much smaller than those measured, particularly in the region of $\rho > 0.5$. The neoclassical estimation cannot explain the large negative electric field.

Before going to examine the nonclassical component, we note the dependence of Γ_j on E_r. Figure 2 shows that the derivative of Γ with respect to E_r, $\partial\Gamma/\partial E_r$, is large for ions, but remains small for electrons. This indicates that the additional electron flux (which is bipolar), if there is any left, is not effective in affecting the solution of E_r. On the contrary, the change of Γ_i by a factor of few would change the solution. Since $\partial\Gamma/\partial E_r$ is much larger for ions than electrons, the relation $\Gamma_i \simeq 0$ is a good approximate form in determining E_r. An additional-bipolar ion fluxes $\Delta\Gamma$ is estimated by the relation

$$\Delta\Gamma_i \simeq -\Delta E \cdot \partial\Gamma_i^{NC(as)}/\partial E_r \qquad (18)$$

where ΔE represents the difference of E_r between the neoclassical calculation and the experimental results.

We study the effects of additional ion loss fluxes, Eqs. (5), (7), and (9) mentioned in §3, and compare theoretical estimation of E_r with those in experiments.

Let us estimate E_r by imposing the following ambipolarity conditions:

$$\Gamma_e^{NC} = \Gamma_i^{NC} \qquad (19\text{-a})$$

$$\Gamma_e^{NC} = \Gamma_i^{NC} + \Gamma_i^{orbit} \qquad (19\text{-b})$$

$$\Gamma_e^{NC} = \Gamma_i^{NC} + \Gamma_{fcx} \qquad (19\text{-c})$$

$$\Gamma_e^{NC} = \Gamma_i^{NC} + \Gamma_i^{orbit} + \Gamma_{fcx} + \Gamma_{icx} \qquad (19\text{-d})$$

In order to see the importance of the additional terms, solutions of Eq.(19-a) to (19-d) are illustrated in Fig.3A for the low density case and in Fig.3B for the high density case. In Figs. 3A and 3B, the curves (a) to (d) represents the radial profiles of E_r as is calculated by the relations (19-a) to (19-d), respectively. Open and closed data points are experimental values, which are quoted from Ref.[29]. In solving these equations, we take r_*=0.6a. This choice of r_* is not affected much for the solution which is obtained in Fig.3. Therefore the constant r_* approximation is a good one. We also take f_{bound} to be unity, in order to estimate the upper bound of the influence of the fast ion orbit loss. Coefficients μ_{i1} and μ_{i2} are chosen as 1.365 and 2.31, respectively.

Figure 3 shows that the fast ion losses which are caused by the loss cone and cx with neutrals are always positive and make the electric field more negative. First, we see that the orbit loss makes the raidal electric field more negative. We would like to note that the influence of the orbit loss appears only in the region r > 0.9a, although, the loss cone is introduced in the region r > r_* and r_*=0.6a. The charge exchange loss of fast particle can also be effective in enhancing the electric field. Predictions by theory approaches to the experimental one. The maximum radial electric field, which is more than five times larger than the neoclassical prediction, exceeds -150eV/cm, approaching the level of the experimental observation. However, the influence is localized near the edge and is still insufficient. As for the contribution of the charge exchange of

bulk ions is concerned, the effect is small. The corrections to the neoclassical prediction is given near the periphery, $r>0.8a$, and is still insufficient. The experimental observations show that E_r substantially deviates from the neoclassical prediction in the region of $r>0.6a$. Based on these results, we see that another bipolar ion loss flux, which is several times as large as the neoclassical one, is necessary to explain this discrepancy.

§5 Summary and Discussions

In this paper, we discussed an analytical modelling of the effect of the nonclassical losses on the radial electric field in torsatron/heliotron configurations. We examined the loss cone loss of fast ions, the loss of fast ions through charge exchange, and the bulk ion loss due to the charge exchange. Applications are made on the NBI plasma in CHS device, in which the radial electric field has been deduced from the measurements of the plasma flows. Comparison was made between the theoretical calculation and experimental one.

We confirmed that both of the orbit loss and charge exchange loss gave a more negative E_r than the neoclassical prediction. Enhancement of the radial electric field is largest near the plasma edge. Although this qualitative agreement was found , the quantitative prediction is not satisfactory. First, E_r deviates from neoclassical theory in the region of $r>0.5a$, while the fast particle effect is only effective in the region of $r>0.8a$. Some other large ion loss process, which is several times as large as the neoclassical one, is necessary in the region of $0.5a<r<0.8a$ to explain the discrepancy between theoretical and experimental results. Unfortunately, the direct comparison cannot be made in the region of $r > 0.8a$, where the experimental observation is not available, although the largest deviation from the neoclassical prediction was found in this article. Even though the absolute value is different, the density dependence of the radial electric field is recovered by this theoretical model. The experiment shows that the edge electric field seems to increase (i.e., is

more negative) as the density increases. The present analysis predicts that E_r becomes more negative as the density increases. This theoretical trend is associated with the fact that the temperature decreases for the higher density.

It should be carefull in comparing theory and experiments on E_r, because E_r has θ dependence due to the ellipticity of the magnetic surface. This correction, however, amounts to about 30% and is not enough to explain the discrepancy. It should be also noted that the solution of Eqs.(19-c) and (19-d) depends on the choice of the neutral density profile, for which good experimental value is not given. Even though this uncertainty cannot be annihilated, the conclusion is not changed so long as the majority of neutrals are supplied by the recycling at the wall, and entering into the core plasma with the energy of the order of a few electron volt. For instance, if we multiply n_{0s} by a factor of 10 (which is beyond the experimental uncertainty), the noticiable deviation from experimental value of E_r still remains. Another possibility to reduce the discrepancy is that neutrals are supplied with much faster speed from the wall so that α_0 is of the order of unity. [In this case, however, the particle confinement time is much underestimated; less than ms at the center.] Further experimental information would be necessary to get rid of this uncertainty.

A satisfactory explanation awaits further theoretical and experimental studies, including the anomalous transport in the whole plasma region.

Acknowledgements

One of the authors (HS) thanks Professor K. L. Kovrizhnykh, who kindly supplied the revised neoclassical transport formula in Ref.[14]. New formula is applicable to the hollow density distributions. We wish to acknowledge Dr. K. Matsuoka and the CHS group for their stimulating discussions. This work is partly supported by the Grant-in-Aid for Scientific Research of MoE Japan.

Appendix: Derivation of Eq.(5)

In this article we assume that the particles are lost if they reach the outermost magnetic surface r=a. A radius $r=r_*$ is defined as follows; the birth particles at the region with $r>r_*$ enter the loss cone, but the particles which ionize at $r<r_*$ do not enter the loss cone. If we introduce the birth rate S(r) [number/m^3s] of the fast ions which are ionized at the position r, the loss flux of fast ions is given as

$$\Gamma^{orbit} = \frac{1}{4\pi^2 Rr}\int_0^{2\pi}\int_0^{2\pi R}\int_0^{r} d\theta r' dr' S(r') p(r';\lambda) dz \qquad (A1)$$

where $p(r;\lambda)$ represents the probability for the particles to enter the loss cone and λ represents the pitch angle of the birth particle. We take a simplification that the pitch angle distribution is a delta function, namely, p(r)=1 for $r>r_*$ and p(r)=0 for $r<r_*$. [The loss boundary r_* is determined by the implicit function including the particle energy, ε_t, $\varepsilon_h(r)$ and the electric field structure, which is given in Ref.[23].]

By this assumption, fast particles with given pitch angle which are born in the region $r_*<r<r_1$ contributes to the radial current at $r=r_1$. The rate of the fast particle generation in the region $r_*<r<r_1$ is given as

$$[P(r_1)-P(r_*)]/E_b \qquad (A2)$$

where P(r) is the injection power across the minor radius r. Thus we obtain

$$\Gamma^{orbit} = \frac{1}{4\pi^2 Rr}\frac{(P(r)-P(r_*))}{E_b} \qquad (A3)$$

When $|r-r_*| \ll a$ holds, $P(r)-P(r_*)$ can be approximated as

$$P(r)-P(r_*) \simeq \left(\frac{r-r_*}{a-r_*}\right)\cdot f_{bound}\cdot P_{in} \qquad (A4)$$

where f_{bound} means the fraction of the absorption power in the region of $r_* < r < a$. The coefficient f_{bound} is less than unity and an increasing function of n_e. Finally, we obtain the fast ion loss flux as

$$\Gamma^{orbit} = \frac{1}{4\pi^2 Rr}\frac{P_{in}}{E_b}\left(\frac{r-r_*}{a-r_*}\right)f_{bound} \qquad (A5)$$

References

[1] F. Wagner, G. Becker, K. Behringer, et al.: Phys. Rev. Lett. **49** (1982) 1408.

[2] J. Groebner, K. H. Burrel and R. P. Seraydarian: Phys. Rev. Lett. **64** (1990) 3015.

[3] K. Ida, S. Hidekuma, Y. Miura, et al: Phys. Rev. Lett. **65** (1990) 1364.

[4] S.-I. Itoh and K. Itoh: Phys. Rev. Lett. **60** (1988) 2276.

[5] H. Sanuki: Phys. Fluids **27** (1984) 2500.

[6] S.-I. Itoh, K. Itoh, T. Ohkawa, et al: in Plasma Physics and Controlled Nuclear Fusion Research 1988, Proc. 12th Int. Conf. Nice, 1988 (IAEA Vienna 1989) Vol.2, p23.

[7] K.C. Shaing, et al: in Plasma Physics and Controlled Nuclear Fusion Research 1988, Proc. 12th Int. Conf. Nice, 1988 (IAEA Vienna 1989) Vol.2, p13.

[8] K. C. Shaing and E. C. Crume: Phys. Rev. Lett. **63** (1989) 2369.

[9] S.-I. Itoh and K. Itoh: J. Phys. Soc. Jpn. **59** (1990) 3815.

[10] H. Sugama and M. Wakatani: Phys. Fluids **B3** (1991) in press.

[11] S.-I. Itoh, H. Sanuki, and K. Itoh: "Effect of Electric Field Inhomogeneities on Drift Wave Instabilities and Anomalous Transport", Research Report NIFS-72 (1991).

[12] R. J. Taylor, M. L. Brown, B. D. Fried, et al.: Phys. Rev. Lett. **63** (1989) 2365.

[13] R. R. Weynants and R. J. Taylor: Nucl. Fusion **30** (1990) 945.

[14] L. M. Kovrizhnykh: Nucl. Fusion **24** (1984) 435.

[15] D. E. Hastings, W. A. Houlberg and K. C. Shaing: Nucl. Fusion **25** (1985) 445.

[16] H. Wobig, H. Maassberg, H. Renner, The WVII-A Team: in

Plasma Physics and Controlled Nuclear Fusion Research 1986, Proc. 11th Int. Conf. Kyoto, 1986 (IAEA Vienna 1987) Vol.2, p369.

[17] K. Kondo, H. Zushi, S. Nishimura, et al: Rev. Sci. Instrum. **59** (1988) 1533.

[18] K. Matsuoka, S. Kubo, M. Hosokawa, et al.: in Plasma Physics and Controlled Nuclear Fusion Research 1988, Proc. 12th Int. Conf. Nice, 1988 (IAEA Vienna 1989) Vol.2, p411.

[19] K. Ida, H. Yamada, H. Iguchi, et al.: Phys. Fluids **B3** (1991) 515.

[20] K. Ida and Hidekuma: Rev. Sci. Instr. 60 (1989) 876.

[21] K. Ida, K. Itoh, S.-I. Itoh, et al.: in 13th International Conference on Plasma Physics and Controlled Nuclear Fusion Research (Washington, 1990) paper IAEA-CN-53/C-3-3.

[22] K. Ida, H. Yamada, H. Iguchi, K. Itoh and CHS Group: "Observation of Parallel Viscosity in the CHS Heliotron/ Torsatron, Research Report NIFS-70 (1991).

[23] K. Itoh, H. Sanuki, J. Todoroki, et al: Phys. Fluids **B3** (1991) in press.

[24] A. C. Riviere: Nucl. Fusion 11 (1971) 363.

[25] S.-I. Itoh: J.Phys. Soc. Jpn. 59 (1990) 3431.

[26] T. H. Stix, Phys. Fluids 16 (1973) 1260.

[27] K. Itoh, S.I. Itoh: Comments Plasma Phys. Cont. Fusion (1991) in press.

[28] E. Yahagi, K. Itoh, M. Wakatani, Plasma Physics and Controlled Fusion **30** (1988) 1009.

[29] K. Ida, et al: Submitted to Phys. Fluids for erratum of [19].

Table Caption

Table 1: Parameters which characterize the bulk density and temperature. Profiles for two typical discharges in a tangentially injected neutral beam experiment of the CHS device. The definition of these parameters are given by Eqs.(13), (14) and (15). Parameters for neutral and fast particle densities (see Eq.(16) and (17)) are also added.

Figure Captions

Fig. 1 Radial Profiles of the density, ion and electron temperatures (T_i, T_e) are shown for the low density (A) and high density (B) NBI discharges in CHS device.

Fig. 2 Neoclassical ion and electron fluxes (Γ_i^{NC}, Γ_e^{NC}) at $\rho=0.8$ versus radial electric field E_r are illustrated for the high (solid lines) and low (dashed lines) cases. Open circles represent E_r determined from $\Gamma_e^{NC}=\Gamma_i^{NC}$.

Fig. 3 Radial electric field profiles are plotted for the low density case (A) and the high density case (B). The curves (a) to (d) represent $E_r(\rho)$ which are determined by the conditions Eqs. (19-a) to (19-d), respectively. Radial electric field profiles which are measured by CXS are shown by solid and open circles (Quoted from Ref. [29] with correction.)

	NBI (Low-n)	NBI (High-n)		NBI (Low-n)	NBI (High-n)
n_{os} $[1/m^3]$	4×10^{17}	4×10^{17}	$T_e(0)$ [ev]	329.9	195.02
α_0	40	40	T_{es} [ev]	26.65	5.00
n_{fo} $[1/m^3]$	1.0×10^{17}	1.0×17^{17}	α_3	1.5	1.8
α_1	2	2	β_3	0.9152	1.0612
$n(0)$ $[1/m^3]$	1.804×10^{19}	5.563×10^{19}	$T_i(0)$ [ev]	203.1	178.27
n_s $[1/m^3]$	1.043×10^{18}	8.831×10^{17}	T_{is} [ev]	26.70	5.00
ρ_m $(=\frac{r_m}{a})$	0.8097	0.6366	α_4	1.5	1.5
α_2	3.8600	6.4975	β_4	1.1652	1.0007
β_2	1.1	20.5959			

Table 1

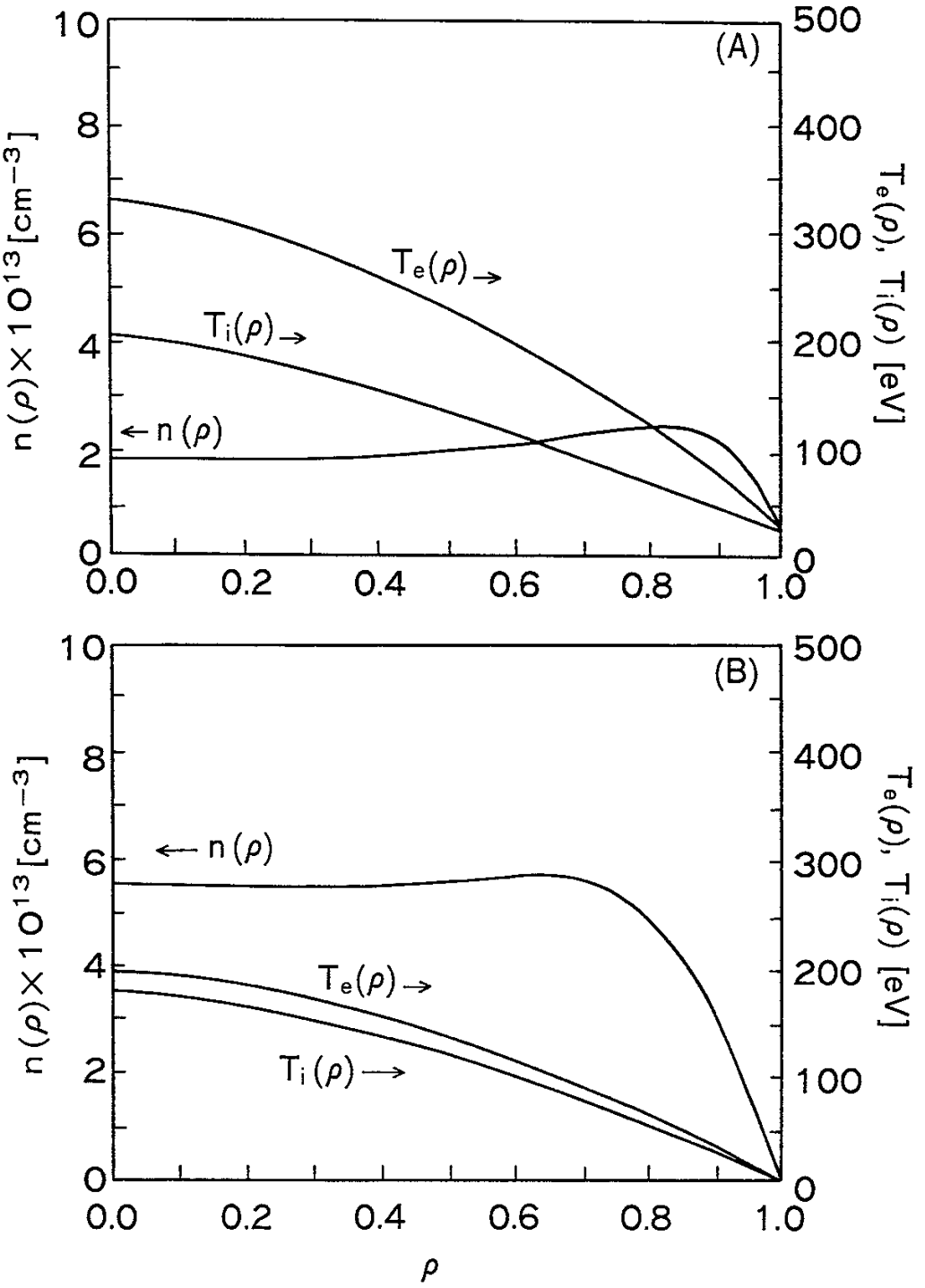
(A)
(B)
$n(\rho) \times 10^{13}$ [cm^{-3}]
$T_e(\rho)$, $T_i(\rho)$ [eV]
$T_e(\rho) \rightarrow$
$T_i(\rho) \rightarrow$
$\leftarrow n(\rho)$
$T_i(\rho) \rightarrow$
ρ

Fig. 1

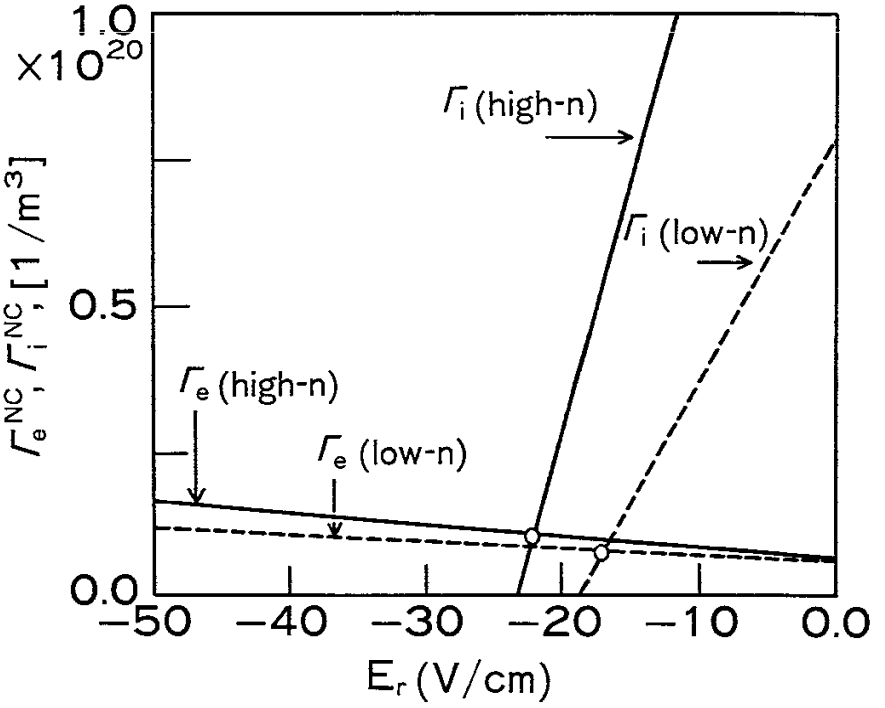
1.0
×10^20
0.5
0.0
Γe^NC, Γi^NC, [1/m^3]
Γi (high-n)
Γi (low-n)
Γe (high-n)
Γe (low-n)
−50
−40
−30
−20
−10
0.0
Er (V/cm)

Fig. 2

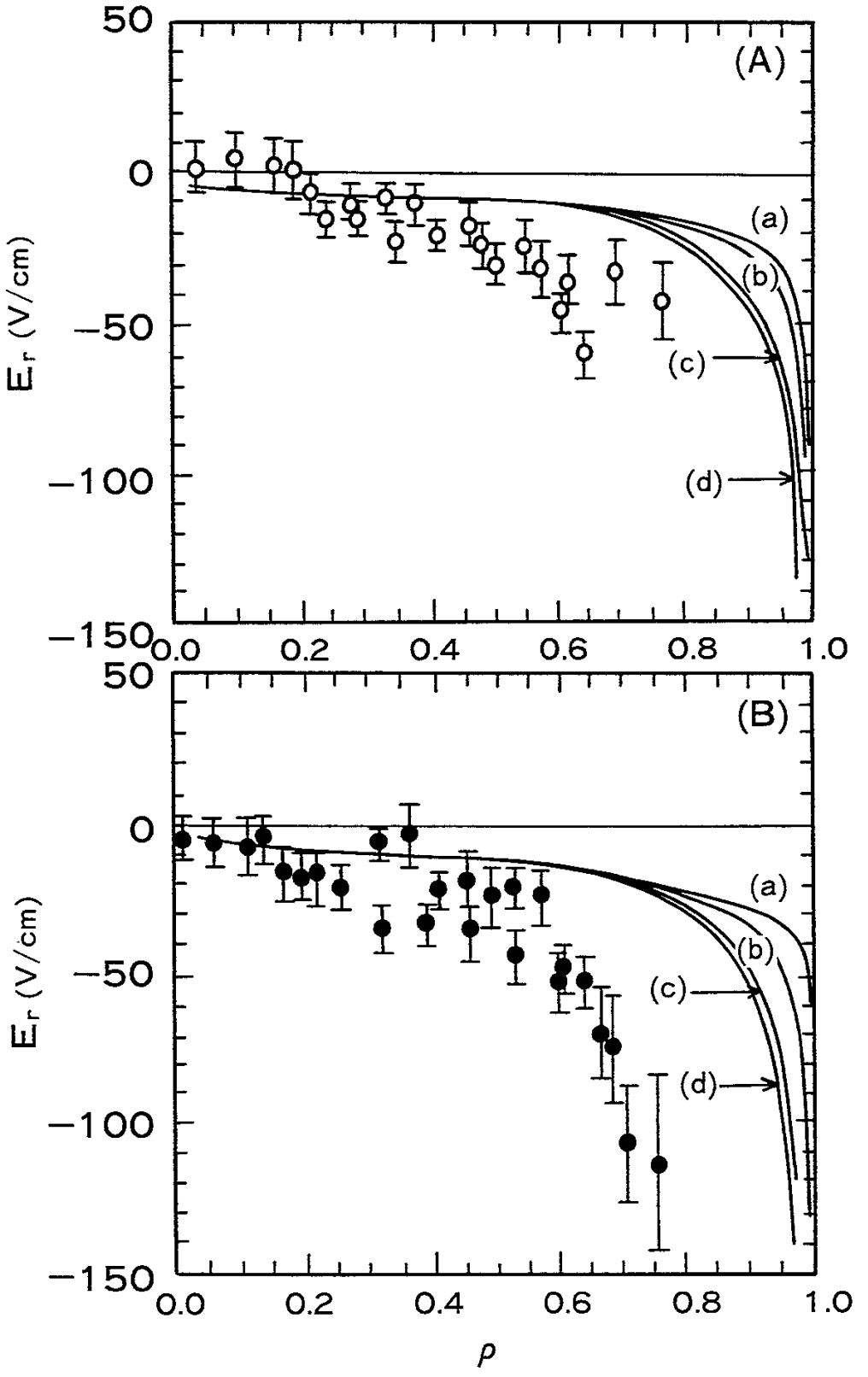

Fig. 3

Recent Issues of NIFS Series

NIFS-41 K. Ida, K. Itoh, S.-I. Itoh, S. Hidekuma and JIPP T-IIU & CHS Group, *Comparison of Toroidal/Poloidal Rotation in CHS Heliotron/Torsatron and JIPP T-IIU Tokamak*; Sep .1990

NIFS-42 T.Watari, R.Kumazawa,T.Seki, A.Ando,Y.Oka, O.Kaneko, K.Adati, R.Ando, T.Aoki, R.Akiyama, Y.Hamada, S.Hidekuma, S.Hirokura, E.Kako, A.Karita, K.Kawahata, T.Kawamoto, Y.Kawasumi, S.Kitagawa, Y.Kitoh, M.Kojima, T. Kuroda, K.Masai, S.Morita, K.Narihara, Y.Ogawa, K.Ohkubo, S.Okajima, T.Ozaki, M.Sakamoto, M.Sasao, K.Sato, K.N.Sato, F.Shinbo, H.Takahashi, S.Tanahashi, Y.Taniguchi, K.Toi, T.Tsuzuki, Y.Takase, K.Yoshioka, S.Kinoshita, M.Abe, H.Fukumoto, K.Takeuchi, T.Okazaki and M.Ohtuka, *,Application of Intermediate Frequency Range Fast Wave to JIPP T-IIU and HT-2 Plasma*; Sep. 1990

NIFS-43 K.Yamazaki, N.Ohyabu, M.Okamoto, T.Amano, J.Todoroki, Y.Ogawa, N.Nakajima, H.Akao, M.Asao, J.Fujita, Y.Hamada, T.Hayashi, T.Kamimura, H.Kaneko, T.Kuroda, S.Morimoto, N.Noda, T.Obiki, H.Sanuki, T.Sato, T.Satow, M.Wakatani, T.Watanabe, J.Yamamoto, O.Motojima, M.Fujiwara, A.Iiyoshi and LHD Design Group, *Physics Studies on Helical Confinement Configurations with l=2 Continuous Coil Systems*; Sep. 1990

NIFS-44 T.Hayashi, A.Takei, N.Ohyabu, T.Sato, M.Wakatani, H.Sugama, M.Yagi, K.Watanabe, B.G.Hong and W.Horton, *Equilibrium Beta Limit and Anomalous Transport Studies of Helical Systems*; Sep. 1990

NIFS-45 R.Horiuchi, T.Sato, and M.Tanaka, *Three-Dimensional Particle Simulation Study on Stabilization of the FRC Tilting Instability*; Sep. 1990

NIFS-46 K.Kusano, T.Tamano and T. Sato, *Simulation Study of Nonlinear Dynamics in Reversed-Field Pinch Configuration*; Sep. 1990

NIFS-47 Yoshi H.Ichikawa, *Solitons and Chaos in Plasma*; Sep. 1990

NIFS-48 T.Seki, R.Kumazawa, Y.Takase, A.Fukuyama, T.Watari, A.Ando, Y.Oka, O.Kaneko, K.Adati, R.Akiyama, R.Ando, T.Aoki, Y.Hamada, S.Hidekuma, S.Hirokura, K.Ida, K.Itoh, S.-I.Itoh, E.Kako, A. Karita, K.Kawahata, T.Kawamoto, Y.Kawasumi, S.Kitagawa, Y.Kitoh, M.Kojima, T.Kuroda, K.Masai, S.Morita, K.Narihara, Y.Ogawa, K.Ohkubo, S.Okajima, T.Ozaki, M.Sakamoto, M.Sasao, K.Sato, K.N.Sato, F.Shinbo, H.Takahashi, S.Tanahashi, Y.Taniguchi, K.Toi and T.Tsuzuki, *Application of Intermediate Frequency Range Fast Wave to JIPP T-IIU Plasma*; Sep.1990

NIFS-49 A.Kageyama, K.Watanabe and T.Sato, *Global Simulation of the Magnetosphere with a Long Tail: The Formation and Ejection of Plasmoids*; Sep.1990

NIFS-50 S.Koide, *3-Dimensional Simulation of Dynamo Effect of Reversed Field Pinch*; Sep. 1990

NIFS-51 O.Motojima, K. Akaishi, M.Asao, K.Fujii, J.Fujita, T.Hino, Y.Hamada, H.Kaneko, S.Kitagawa, Y.Kubota, T.Kuroda, T.Mito, S.Morimoto, N.Noda, Y.Ogawa, I.Ohtake, N.Ohyabu, A.Sagara, T. Satow, K.Takahata, M.Takeo, S.Tanahashi, T.Tsuzuki, S.Yamada, J.Yamamoto, K.Yamazaki, N.Yanagi, H.Yonezu, M.Fujiwara, A.Iiyoshi and LHD Design Group, *Engineering Design Study of Superconducting Large Helical Device*; Sep. 1990

NIFS-52 T.Sato, R.Horiuchi, K. Watanabe, T. Hayashi and K.Kusano, *Self-Organizing Magnetohydrodynamic Plasma*; Sep. 1990

NIFS-53 M.Okamoto and N.Nakajima, *Bootstrap Currents in Stellarators and Tokamaks*; Sep. 1990

NIFS-54 K.Itoh and S.-I.Itoh, *Peaked-Density Profile Mode and Improved Confinement in Helical Systems*; Oct. 1990

NIFS-55 Y.Ueda, T.Enomoto and H.B.Stewart, *Chaotic Transients and Fractal Structures Governing Coupled Swing Dynamics*; Oct. 1990

NIFS-56 H.B.Stewart and Y.Ueda, *Catastrophes with Indeterminate Outcome*; Oct. 1990

NIFS-57 S.-I.Itoh, H.Maeda and Y.Miura, *Improved Modes and the Evaluation of Confinement Improvement*; Oct. 1990

NIFS-58 H.Maeda and S.-I.Itoh, *The Significance of Medium- or Small-size Devices in Fusion Research*; Oct. 1990

NIFS-59 A.Fukuyama, S.-I.Itoh, K.Itoh, K.Hamamatsu, V.S.Chan, S.C.Chiu, R.L.Miller and T.Ohkawa, *Nonresonant Current Drive by RF Helicity Injection*; Oct. 1990

NIFS-60 K.Ida, H.Yamada, H.Iguchi, S.Hidekuma, H.Sanuki, K.Yamazaki and CHS Group, *Electric Field Profile of CHS Heliotron/Torsatron Plasma with Tangential Neutral Beam Injection*; Oct. 1990

NIFS-61 T.Yabe and H.Hoshino, *Two- and Three-Dimensional Behavior of Rayleigh-Taylor and Kelvin-Helmholz Instabilities*; Oct. 1990

NIFS-62 H.B. Stewart, *Application of Fixed Point Theory to Chaotic Attractors of Forced Oscillators;* Nov. 1990

NIFS-63 K.Konn., M.Mituhashi, Yoshi H.Ichikawa,*Soliton on Thin Vortex Filament;* Dec. 1990

NIFS-64 K.Itoh, S.-I.Itoh and A.Fukuyama,*Impact of Improved Confinement on Fusion Research;* Dec. 1990

NIFS -65 A.Fukuyama, S.-I.Itoh and K. Itoh,*A Consistency Analysis on the Tokamak Reactor Plasmas;* Dec. 1990

NIFS-66 K.Itoh, H. Sanuki, S.-I. Itoh and K. Tani,*Effect of Radial Electric Field on α-Particle Loss in Tokamaks;* Dec. 1990

NIFS-67 K.Sato,and F.Miyawaki,*Effects of a Nonuniform Open Magnetic Field on the Plasma Presheath*; Jan.1991

NIFS-68 K.Itoh and S.-I.Itoh,*On Relation between Local Transport Coefficient and Global Confinement Scaling Law;* Jan. 1991

NIFS-69 T.Kato, K.Masai, T.Fujimoto,F.Koike, E.Källne, E.S.Marmar and J.E.Rice,*He-like Spectra Through Charge Exchange Processes in Tokamak Plasmas;* Jan.1991

NIFS-70 K. Ida, H. Yamada, H. Iguchi, K. Itoh and CHS Group, *Observation of Parallel Viscosity in the CHS Heliotron/Torsatron* ; Jan.1991

NIFS-71 H. Kaneko, *Spectral Analysis of the Heliotron Field with the Toroidal Harmonic Function in a Study of the Structure of Built-in Divertor* ; Jan. 1991

NIFS-72 S. -I. Itoh, H. Sanuki and K. Itoh, *Effect of Electric Field Inhomogeneities on Drift Wave Instabilities and Anomalous Transport* ; Jan. 1991

NIFS-73 Y.Nomura, Yoshi.H.Ichikawa and W.Horton, *Stabilities of Regular Motion in the Relativistic Standard Map*; Feb. 1991

NIFS-74 T.Yamagishi, *Electrostatic Drift Mode in Toroidal Plasma with Minority Energetic Particles,* Feb. 1991

NIFS-75 T.Yamagishi, *Effect of Energetic Particle Distribution on Bounce Resonance Excitation of the Ideal Ballooning Mode*, Feb. 1991

NIFS-76 T.Hayashi, A.Tadei, N.Ohyabu and T.Sato, *Suppression of Magnetic Surface Breading by Simple Extra Coils in Finite Beta Equilibrium of Helical System;* Feb. 1991

NIFS-77 N. Ohyabu, *High Temperature Divertor Plasma Operation*; Feb. 1991

NIFS-78 K.Kusano, T. Tamano and T. Sato, *Simulation Study of Toroidal Phase-Locking Mechanism in Reversed-Field Pinch Plasma*; Feb. 1991

NIFS-79 K. Nagasaki, K. Itoh and S. -I. Itoh, *Model of Divertor Biasing and Control of Scrape-off Layer and Divertor Plasmas*; Feb. 1991

NIFS-80 K. Nagasaki and K. Itoh, *Decay Process of a Magnetic Island by Forced Reconnection*; Mar. 1991

NIFS-81 K. Takahata, N. Yanagi, T. Mito, J. Yamamoto, O.Motojima and LHDDesign Group, K. Nakamoto, S. Mizukami, K. Kitamura, Y. Wachi, H. Shinohara, K. Yamamoto, M. Shibui, T. Uchida and K. Nakayama, *Design and Fabrication of Forced-Flow Coils as R&D Program for Large Helical Device*; Mar. 1991

NIFS-82 T. Aoki and T. Yabe, *Multi-dimensional Cubic Interpolation for ICF Hydrodynamics Simulation*; Apr. 1991

NIFS-83 K. Ida, S.-I. Itoh, K. Itoh, S. Hidekuma, Y. Miura, H. Kawashima, M. Mori, T. Matsuda, N. Suzuki, H. Tamai, T.Yamauchi and JFT-2M Group, *Density Peaking in the JFT-2M Tokamak Plasma with Counter Neutral Beam Injection* ; May 1991

NIFS-84 A. Iiyoshi, *Development of the Stellarator/Heliotron Research*; May 1991

NIFS-85 Y. Okabe, M. Sasao, H. Yamaoka, M. Wada and J. Fujita, *Dependence of Au^- Production upon the Target Work Function in a Plasma-Sputter-Type Negative Ion Source;* May 1991

NIFS-86 N. Nakajima and M. Okamoto, *Geometrical Effects of the Magnetic Field on the Neoclassical Flow, Current and Rotation in General Toroidal Systems*; May 1991

NIFS-87 S. -I. Itoh, K. Itoh, A. Fukuyama, Y. Miura and JFT-2M Group, *ELMy-H mode as Limit Cycle and Chaotic socillations in Tokamak Plasmas;* May 1991

NIFS-88 N.Matsunami and K.Kitoh, *High Resolution Spectroscopy of H^+ Energy Loss in Thin Carbon Film;* May 1991

NIFS-89 H. Sugama, N. Nakajima and M.Wakatani, *Nonlinear Behavior of Multiple-Helicity Resistive Interchange Modes near Marginally Stable States;* May 1991

NIFS-90 H. Hojo and T.Hatori, *Radial Transport Induced by Rotating RF Fields and Breakdown of Intrinsic Ambipolarity in a Magnetic Mirror*; May 1991

NIFS-91 M. Tanaka, S. Murakami, H. Takamaru and T.Sato, *Macroscale Implicit, Electromagnetic Particle Simulation of Inhomogeneous and Magnetized Plasmas in Multi-Dimensions;* May 1991

NIFS-92 S. - I. Itoh, *H-mode Physics, -Experimental Observations and Model Theories-, Lecture Notes, Spring College on Plasma Physics, May 27 - June 21 1991 at International Centre for Theoretical Physics (IAEA UNESCO) Trieste, Italy ;* Jun. 1991

NIFS-93 Y. Miura, K. Itoh, S. - I. Itoh, T. Takizuka, H. Tamai, T. Matsuda, N. Suzuki, M. Mori, H. Maeda and O. Kardaun, *Geometric Dependence of the Scaling Law on the Energy Confinement Time in H-mode Discharges;* Jun. 1991